

Silica botryoids from chemically oscillating reactions and as Precambrian environmental proxies

Shahab Varkouhi¹ and Dominic Papineau^{1,2}

¹ Department of Earth Sciences, University College London, London, UK

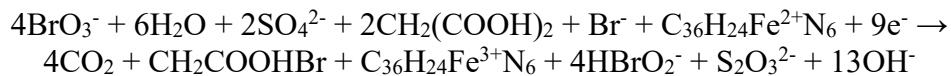
² London Centre for Nanotechnology, University College London, London, UK

ABSTRACT

In this petrographic and geochemical study, we differentiate diverse quartz botryoids, including circular-concentric, twinned, columnar, wavy, and stromatolite-like structures versus synchronous biotic patterns of similar geometry and size dimensions (filamentous traits and stromatolites) in Precambrian cherts of Barberton, South Africa and Gunflint, Canada. The botryoidal habits explored retain self-similar patterns of radially aligned acicular quartz with concentric laminae, which is not documented in biologically built stromatolites. These ancient fractals and their composition imitate those in the chemically oscillating reactions (COR), implying that the precipitation of botryoids was fueled by abiotic diagenetic degradation of organic matter (OM) and subsequently metamorphosed into chert.

INTRODUCTION

Interrogation of botryoidal mineral habits, displaying circularly concentric and radial geometries, in Precambrian cherts has been motivated because of the potential to retain organic matter (OM) in their texture (Papineau et al., 2021). The occurrence of silica botryoids consists with microbial metabolic pathways, as these patterns likely form in organic-acid rich media (Varkouhi et al., 2022). However, the absence of certain biosignatures, such as fossils and ¹³C-depleted OM, in very ancient strata questions the biogenicity of botryoids for tracing the earliest life signatures (Schopf, 2006). Quartz botryoids in Paleoproterozoic chert from Western Australia have concentric laminae akin to those produced by decarboxylation in chemically oscillating reactions (COR), and can thus be linked to abiotic processes (Varkouhi et al., 2022). During COR, the decarboxylation of organic acids by oxidants and strong acids is catalyzed by phenanthroline ferrous sulfate. This phenomenon produces circularly concentric and radially expanding waves along with carbon dioxide and intermediates, including bromomalonic acid and bromine oxoacid:



The diffusion of abiotic COR products forms chemical waves with a fractal habit, self-repeating growth of concentric laminae over multiple orders of dimensions, the destructive interference of which obliterates the wave trace. The COR patterns also simulate younger botryoids, including Ediacaran botryoidal quartz from the aftermath of the Marinoan glaciation (Papineau et al., 2021) and Paleoproterozoic stromatolitic dolomite (Goodwin and Papineau, 2022). While radial fabrics combined with botryoidal and granular chert were reported in the Precambrian of South Africa (Tice and Lowe, 2006) and Canada (Javaux and Lepot, 2018), no research addressed the provenance of these patterns using chemical simulations. Here, we describe periodic geometries in COR experiments, and compare their generated fractals with quartz botryoids in Paleoproterozoic Barberton chert, South Africa (3.26–3.23 Ga; Lowe et al., 2019) and late Paleoproterozoic Gunflint chert, Canada (1.88 Ga; Alleon et al., 2016). A model is proposed that highlights OM in botryoids to track the likely decarboxylation in these Precambrian environments. As COR involve abiotic carbon cycling, botryoids can be linked to sediment records of this cycle, which implies the possibility of using these objects to search for prebiotic organic

traces (Papineau et al., 2023).

MATERIALS AND METHODS

The Barberton chert samples were collected from the Lower Fig Tree and Onverwacht groups of the Barberton Greenstone Belt in the Barite Valley area and the Onverwacht Anticline (Figs. DR1A–C). The outcrop of the Gunflint chert was near the Schreiber locality in Ontario (Figs. DR1D–F). Optical petrography was conducted on thin sections with an Olympus BX-51 microscope. The distribution of OM in minerals was characterized using a WITec Alpha300 Raman spectrometer. The transmitted-light images of laminated patterns produced by COR experiments, including new ones and previous video footage from Papineau (2020) and Papineau et al. (2021) were used for comparison with fractals in chert botryoids. The operating conditions for petrographic analyses and COR experiments are described in the GSA Data Repository.

SHALLOW-MARINE DEPOSITIONAL FRAMEWORK

Within the Fig Tree Group (3260–3225 Ma), the chert and turbiditic basal sequence of the Mapepe Formation overlies the chert dikes of the Mendon Formation (Onverwacht Group; 3335–3260 Ma; Byerly et al., 1996; Fig. DR1B). This ~10-m-thick shallow-water sequence comprises distinct chert layers ~0.5 m in thickness with botryoids (Fig. 1; Figs. DR2A–F) and is conformably succeeded by 100–200 m of felsic pyroclastics. The sequence hosts traces of microbially depleted 34S, which are among the earliest chemical biosignature (Roerdink et al., 2013). Below the Mendon Formation, the ~350-m-thick Buck Reef Chert marks the stratigraphic transition from the banded chert base of the Kromberg Formation to the underlying mainly basaltic Hooggenoeg Formation.

The Gunflint chert occurs within the Gunflint Range along the northern coast of Lake Superior, and continues to crop out beyond the Gunflint Range onto the district of Schreiber (Figs. DR1D–F). Within the Proterozoic metasediment, the Gunflint Formation with 120 m of clastic, carbonate, and stromatolitic chert (Fralick et al., 2002) rests conformably on marine sandstones, and is overlain by argillite. While the base of Gunflint chert is marked by granules with coccoidal and filamentous microfossils (Papineau et al., 2017; Figs. DR2G–J), which indicate the interior zone of a tidal platform (Wacey et al., 2012), the upper part incorporates the distribution of botryoids (Fig. 1).

FRACTAL PATTERNS IN B-Z REACTIONS AND QUARTZ BOTRYOIDS

In the B-Z experiment, fractals produced by the periodic diffusion of reaction products commonly consist of circularly concentric and equidistant waves along with cavity-shaped intersections (Figs. 2I–III). Long-period first-order fluctuations between orange-red and purple-blue phases (several mins) and short-period second-order 0.1–10 cm circular waves (over ~1 min) were generated by radial growth of oscillations. Oscillation of a spotted background with a fast-period (third-order 0.1–1 mm spots over ~20 sec), distinct from the second-order waves as sub-millimetric oxidation spots, was occasionally characterized in COR. The circular oscillations produced twinned patterns from destructive interference of propagating waves (Figs. 2II, III). Nevertheless, a spectrum of other fractals, including stromatolite-like forms (Figs. DR3A–C), unrolled wavy and parallel laminae (Figs. DR3D, E), concentric elliptical shapes (Figs. DR3F–H), rosette-like features (Figs. DR3G, I), and spiral patterns (Figs. DR3B–D, F) variably occurred. Very similar geometry of stromatolite-like/stromatolite (Figs. 3I, II; Figs. DR2H–J), circular-concentric (Fig. 1I; Figs. 3III, IV), cavity-shaped (Fig. 1II; Figs. DR2A, B, E, F), twinned (Fig. 1III), and wavy laminae (Fig. 3V) also occurs in the Barberton and Gunflint cherts. Excluding the stromatolitic, wavy, and filamentous patterns of cryptocrystalline silica (Figs. 3II, V, VI; Figs. DR2H–J), these fabrics combine radial acicular quartz with laminated concentricity (e.g., Fig. 1I).

ORGANIC MATTER IN BARBERTON AND GUNFLINT CHERT

Raman spectra for OM in quartz botryoids of the Barberton chert display high-intensity D1 and G bands at 1347–1353 and 1603–1613 cm⁻¹, respectively (Figs. 3I, III, V), however OM was not detected in the accessory sulfides and Fe-oxides associated with the botryoidal fabric (Fig. 3VII). In the Gunflint chert,

while filamentous patterns and stromatolites display marked dissemination of OM peaked at 1342–1343 and 1608–1609 cm⁻¹ (D1 and G bands), concentric botryoidal laminae contain no OM (Fig. 3IV). Secondary minerals in the botryoidal microtexture enclose only small fractions of OM, marked by low-intensity peaks 1330 and 1609 cm⁻¹ (D1 and G bands) associated with ankerite in the Gunflint chert (Fig. 3VIII). The crystallization temperature of OM in the Gunflint chert calculated using Lorentz-fitted D1–D4 and G bands varies from 209 to 357 °C (286±51 °C, the mean; Figs. DR4A, B; Table DR1). These spectrally derived temperatures are close to previous average estimates of 262±77 °C for the Gunflint chert, which conform to metamorphism at the prehnite-pumpellyite to lower greenschist facies (Alleon et al., 2016; Papineau et al., 2017). The model-calculated OM metamorphic temperature for the Barberton chert varies from 184 to 238 °C (Table DR1; Figs. DR4C, D), which is consistent with former temperature ranges of ~200–300 °C for that chert, also complying with prehnite-pumpellyite to lower greenschist grade metamorphism (Tice et al., 2004; Alleon et al., 2021).

CHEMICALLY OSCILLATING REACTIONS – IMPLICATIONS FOR CHEMISTRY OF PORE WATER PRECIPITATING SILICA BOTRYOIDS

Self-repeating quartz botryoids with geometry and dimensions imitating those in COR (Fig. 1; Fig. 2; Fig. DR2; Fig. DR3) suggest that the underlying process is the same in regulating their formation. In COR, substantial CO₂ is visibly produced and the volatile products of degraded metabolites, such as malonic acid and aspartic acid, accelerate silica precipitation by lowering the pH. Analogously, wave propagation from oxidation spots was possibly immobilized at solubility equilibrium after exhaustion of reactants, triggering silica precipitation from the pore water as circular botryoids of radial quartz fabric (e.g., Fig. 1I). As COR lower the alkalinity of silica-bearing pore water, the drop in pH due to decarboxylation would trigger permineralization in silica (Papineau et al., 2021). Experimental precipitation of chemical oscillations in reactions with silica polyacrylamide and nanocomposites retains chemical waves in solid states (Chen et al., 2011). This scenario is also acknowledged by the appearance of irregular rosettes and spiral patterns (Figs. DR3B–D, F, G, I) from growth of incipient oxidation spots as convoluted concentric traits. Because different COR reactants used here and in former research (e.g., Orbán et al., 2001) generate various concentric laminae, multiple botryoids in the examined cherts imply that these reactants were mostly present during diagenesis to form the fractals. Pore-water oxidation of carboxyl-rich biomass by sulfate, ferrihydrite, and oxidized halogens produces bicarbonate that precipitates as carbonate minerals, hydrogen sulfide that becomes pyrite and chalcocite, and ferric-ferrous oxides that form hematite and goethite (Papineau et al., 2017). Following observations from diagenetic experiments (e.g., Köhler et al., 2013), the oxidation of OM should produce Fe(II)-minerals. Thus, the absence of OM in some Gunflint botryoids and association of Barberton chert with Fe-oxides could possibly be the result of late oxidation of Fe(II)-minerals. Variably detected dissemination of Fe²⁺-rich hematite, Fe-oxyhydroxides, OM, and chalcocite in the Barberton chert (Fig. 1I; Fig. 3VII; Figs. DR2A–F) as well as ankerite in the Gunflint chert (Fig. 3VIII) support the COR pathway for the formation of botryoidal quartz.

PROVENANCE AND FATE OF ORGANIC MATTER IN QUARTZ BOTRYOIDS

The botryoidal textures are ascribed to the decarboxylation-induced precipitation of colloidal quartz, implying that their OM content is authigenic and syngenetic. Lorentz peak fits propose disordered patterns partly comprising weakly resolved D2–D4 bands, indicative of various molecular functional groups, for the Gunflint chert OM (Figs. DR4A, B). The analogy of spectrally derived temperatures here (Table DR1) and former estimates (200–300 and 199–346 °C for Barberton and Gunflint cherts, respectively) suggests degradation of the botryoidal OM at metamorphic temperatures below 350 °C. Along with the retained fabric incorporating radial quartz with concentric laminae, these temperatures accord with the prehnite-pumpellyite to lower greenschist facies and weak crystallization of graphite (resolved G and D1 bands). The systematically preserved OM in the botryoid (Fig. 3) can be related to the residues of oxidized organic acids from putrefied biomass (Boyd, 2001), which produced laminae imitated by COR waves. Plausibly, pervasive introduction of bitumen in the Gunflint Formation could have infiltrated the botryoidal chert (Rasmussen et al., 2021). However, the growth of botryoids could

still be coeval with OM emplacement, as OM disseminations are associated with botryoids by circular concentricity. Also, the OM molecular structure alters even under low-grade metamorphism (Boudou et al., 2008) so that the OM in botryoids cannot be simply attributed to biotic origins. Moreover, the concentric laminae with radial fabrics differentiate the botryoid and COR versus synchronous stromatolites documented in the same chert but consistent with microbial substrates (e.g., Figs. DR2H–J). The organic molecules, including alkanolic acids produced abiotically via hydrogenation of inorganic carbon in Fischer-Tropsch Type (FTT) reactions constitute an abiotic model for carbon cycling in prebiotic chemistry (McCollom et al., 1999), although microbial build-ups are also retained in ancient cherts (Allwood et al., 2009).

QUARTZ BOTRYOIDS — AN ABIOTIC GROWTH MODEL

The consistent geometry of COR-produced fractals combined with the composition of reactants in COR imply that the abiotic degradation of biomass can trigger the precipitation of colloidal silica into quartz botryoids (Figs. 4A–D). Oxidized bromate or iodate, and other oxidants, such as perchlorate-chlorite (Belmonte et al., 1997) and chlorate–iodine (Sant’Anna and Faria, 2014) systems can decarboxylate the OM and could become concentrated during diagenetic dehydration. Dissemination of Fe-oxides in the OM-rich botryoids, including those with circular and twinned habits (e.g., Fig. 1I) signifies variations in metal oxidation states in the oxidizing solution, consistent also with abiotic sulfate reduction during decarboxylation (Figs. 4A, B). These nanoscopic precipitates are thus modeled as mineralized botryoidal habits that exhibit many of the same patterns in COR. This model here applied to the Barberton and Gunflint cherts conforms to abiogenicity of other spheroidal features, including granules, nodules, and carbonate botryoids elsewhere in the Proterozoic and older rocks (Papineau et al., 2016, 2017; Dodd et al., 2018; Papineau et al., 2021, 2022; Varkouhi et al., 2022). The model grants a specific class of reaction to the origin of botryoidal growth patterns, such as regularly circular laminae and their syngenetic unrolled columnar features (Figs. 3III, IV; Figs. DR2C, D). These patterns imply precipitation of concentric waves under lowered alkalinity at silica solubility equilibrium when abiotic COR decarboxylated the OM (Figs. 4C, D). The model does not rule out the biogenicity of analogous features in these cherts, including the biological origin of microstromatolites.

CONCLUSIONS

The Barberton and Gunflint nearshore Precambrian cherts preserve quartz botryoids, including circularly concentric, cavity-shaped, twinned, wavy, and stromatolite-like laminated patterns formed synchronously with microbial stromatolites and filamentous microfossils. The compelling resemblance of fractals and of the chemistry of solutions in botryoidal quartz precursor and in COR experiments point to their common generation from abiotic decarboxylation of OM. The botryoids are hereupon modeled as mineralized habits of self-oscillating chemical waves formed when inorganic acids and oxidizers degraded carboxylic acids. Although solid silica botryoids have not been generated in COR experiments, they co-occur with diverse biogenic signatures, which implies their potential as abiotic biosignatures involving the putrefaction of biomass. The consistency of botryoidal precipitates with abiotic sources underlined here and in former works implicates the prospect of utilizing these ancient compositions to trace the signature of extra-terrestrial life.

ACKNOWLEDGMENTS

We would like to thank the editor and the two anonymous reviewers for their constructive reviews.

REFERENCES CITED

Alleon, J., Bernard, S., Le Guillou, C., Marin-Carbonne, J., Pont, S., Beyssac, O., McKeegan, K.D., and Robert, F., 2016, Molecular preservation of 1.88 Ga Gunflint organic microfossils as a function of temperature and mineralogy: *Nature Communications*, v. 7, 11977.

Alleon, J., Bernard, S., Olivier, N., Thomazo, C., and Marin-Carbonne, J., 2021, Inherited geochemical diversity of 3.4 Ga organic films from the Buck Reef Chert, South Africa: *Communications Earth &*

Environment, v. 2, 6.

Allwood, A.C., Grotzinger, J.P., Knoll, A.H., Burch, I.W., Anderson, M.S., Coleman, M.L., and Kanik, I., 2009, Controls on development and diversity of Early Archean stromatolites: Proceedings of the National Academy of Sciences, v. 106, p. 9548–9555.

Belmonte, A., Ouyang, Q., and Flesselles, J.M., 1997, Experimental survey of spiral dynamics in the Belousov-Zhabotinsky reaction: *Journal de Physique II*, v. 7, p. 1425–1468.

Boudou, J.-P., Schimmelmann, A., Ader, M., Mastalerz, M., Sebito, M., and Gengembre, L., 2008, Organic nitrogen chemistry during low-grade metamorphism: *Geochimica et Cosmochimica Acta*, v. 72, p. 1199–1221.

Boyd, S.R., 2001, Nitrogen in future biosphere studies: *Chemical Geology*, v. 176, p. 1–30.

Byerly, G.R., Kröner, A., Lowe, D.R., Todt, W., and Walsh, M.M., 1996, Prolonged magmatism and time constraints for sediment deposition in the early Archean Barberton greenstone belt: Evidence from the Upper Onverwacht and Fig Tree groups: *Precambrian Research*, v. 78, p. 125–138.

Chen, I., Kuksenok, O., Yashin, V.V., Moslin, R.M., Balazs, A.C., and Van Vliet, K.J., 2011, Shape- and size-dependent patterns in self-oscillating polymer gels: *Soft Matter*, v. 7, p. 3141–3146.

Dodd, M.S., Papineau, D., She, Z., Fogel, M.L., Nederbragt, S., and Pirajno, F., 2018, Organic remains in late Palaeoproterozoic granular iron formations and implications for the origin of granules: *Precambrian Research*, v. 310, p. 133–152.

Fralick, P., Davis, D.W., and Kissin, S.A., 2002, The age of the Gunflint Chert, Ontario, Canada: single zircon U–Pb age determinations from reworked volcanic ash: *Canadian Journal of Earth Sciences*, v. 39, p. 1085–1091.

Goodwin, A., and Papineau, D., 2022, Biosignatures associated with organic matter in late Paleoproterozoic stromatolitic dolomite and possible implications for Martian carbonates: *Astrobiology*, v. 22, p. 49–74.

Javaux, E.J., and Leptot, K., 2018, The Paleoproterozoic fossil record: Implications for the evolution of the biosphere during Earth's middle-age: *Earth-Science Reviews*, v. 176, p. 68–86.

Köhler, I., Konhauser, K., Papineau, D., Bekker, A., and Kappler, A., 2013, Biological carbon precursor to diagenetic siderite with spherical structures in iron formations: *Nature Communications*, v. 4, 1741.

Lowe, D.R., Drabon, N., and Byerly, G.R., 2019, Crustal fracturing, unconformities, and barite deposition, 3.26–3.23 Ga, Barberton Greenstone Belt, South Africa: *Precambrian Research*, v. 327, p. 34–46.

McCollom, T.M., Ritter, G., and Simoneit, B.R.T., 1999, Lipid synthesis under hydrothermal conditions by Fischer-Tropsch-Type Reactions: *Origins of Life and Evolution of the Biosphere*, v. 29, p. 153–166.

Orbán, M., Kurin-Csörgei, K., Zhabotinsky, A.M., and Epstein, I.R., 2001, A new chemical system for studying pattern formation: Bromate-hypophosphite-acetone-dual catalyst: *Faraday Discussion*, v. 120, p. 11–19.

Papineau, D., De Gregorio, B.T., Fearn, S., Kilcoyne, D., Purohit, R., and Fogel, M.L., 2016, Nanoscale

petrographic and geochemical insights on the origin of Paleoproterozoic stromatolitic phosphorites from Aravalli, India: *Geobiology*, v. 14, p. 3–32.

Papineau, D., She, Z., and Dodd, M.S., 2017, Chemically-oscillating reactions during the diagenetic oxidation of organic matter and in the formation of granules in late Palaeoproterozoic chert from Lake Superior: *Chemical Geology*, v. 470, p. 33–54.

Papineau, D., 2020, Chemically oscillating reactions in the formation of botryoidal malachite: *American Mineralogist*, v. 105, p. 447–454.

Papineau, D., Yin, J., Devine, K., Liu, D., and She, Z., 2021, Chemically oscillating reactions during the diagenetic formation of Ediacaran siliceous and carbonate botryoids: *Minerals*, v. 11, 1060.

Papineau, D., She, Z., Dodd, M.S., Iacoviello, F., Slack, J.F., Hauri, E., Shearing, P., and Little, C. T.S., 2022, Metabolically diverse primordial microbial communities in Earth's oldest seafloor-hydrothermal jasper: *Science Advances*, v. 8, [10.1126/sciadv.abm2296](https://doi.org/10.1126/sciadv.abm2296)

Papineau, D., Devine, K., and Nogueira, B., 2023, Self-similar patterns from abiotic decarboxylation metabolism through chemically oscillating reactions: A prebiotic model for the origin of life: *Life*, v. 13, 551.

Rasmussen, B., Muhling, J.R., and Fischer, W.W., 2021, Ancient oil as a source of carbonaceous matter in 1.88-billion-year-old Gunflint stromatolites and microfossil: *Astrobiology*, v. 21, p. 655–672.

Roerdink, D.L., Mason, P.R.D., Whitehouse, M.J., and Reimer, T., 2013, High-resolution quadruple sulfur isotope analyses of 3.2Ga pyrite from the Barberton Greenstone Belt in South Africa reveal distinct environmental controls on sulfide isotopic arrays: *Geochimica et Cosmochimica Acta*, v. 117, p. 203–215.

Sant'Anna, R.T.P., and Faria, R.B., 2014, The chlorate-iodine-nitrous acid clock reaction: *PLoS ONE*, v. 9, e109899.

Schopf, J.W., 2006, Fossil evidence of Archaean life: *Philosophical Transactions of the Royal Society B: Biological Sciences*, v. 361, p. 869–885.

Tice, M.M., Bostick, B.C., and Lowe, D.R., 2004, Thermal history of the 3.5–3.2 Ga Onverwacht and Fig Tree Groups, Barberton greenstone belt, South Africa, inferred by Raman microspectroscopy of carbonaceous material: *Geology*, v. 32, p. 37–40

Tice, M.M., and Lowe, D.R., 2006, The origin of carbonaceous matter in pre-3.0 Ga greenstone terrains: A review and new evidence from the 3.42 Ga Buck Reef Chert: *Earth-Science Reviews*, v. 76, p. 259–300.

Varkouhi, S., Papineau, D., and Guo, Z., 2022, Botryoidal quartz as an abiotic signature in Palaeoarchean cherts of the Pilbara Supergroup, Western Australia: *Precambrian Research*, v. 383, 106876.

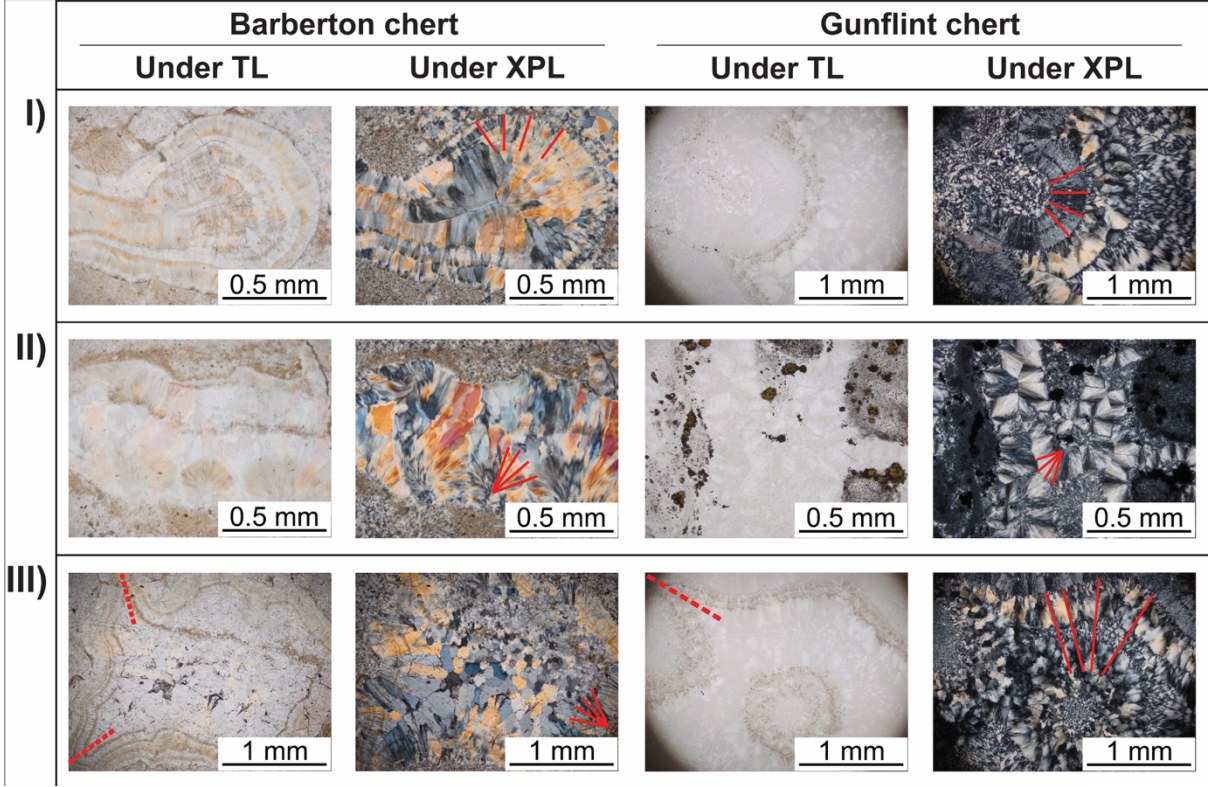
Wacey, D., Menon, S., and Green, L., Gerstmann, D., Kong, C., McLoughlin, N., Saunders, M., and Brasier, M., 2012, Taphonomy of very ancient microfossils from the ~3400 Ma Strelley Pool Formation and ~1900 Ma Gunflint Chert: New insights using a focused ion beam: *Precambrian Research*, v. 220, p. 234–250.

Figure 1. Grid of geometries displayed by studied quartz botryoids. I: Circularly concentric and equidistant to irregular laminae with disseminated hematite. II: Cavity structures embedding concentric laminae with radial acicular quartz. III: Cavity-shaped objects produced by twinned wavy laminae. TL = transmitted light, XPL = cross-polarized light, red lines = radial acicular quartz, red dotted lines = traces of twinned waves.

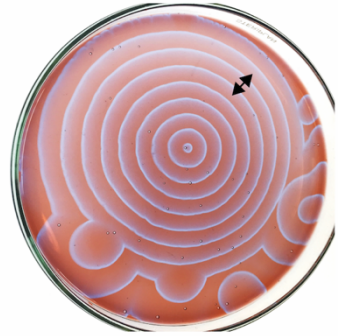
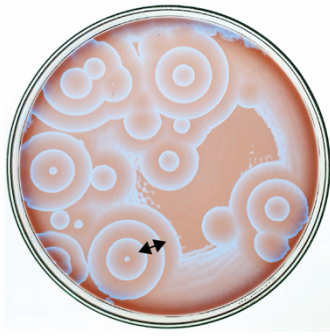
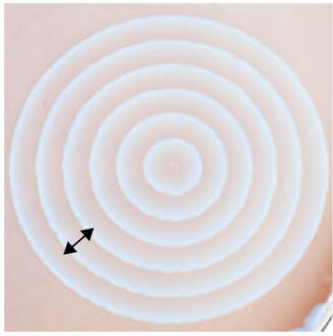
Figure 2. Self-similar patterns generated by selected B-Z experiments (II and III are reprinted after Papineau (2020) and Papineau et al. (2021)). I: Perfect to slightly imperfect circular-concentric equidistant laminae. II: Cavity-shaped structures enclosing equidistant to non-equidistant concentric laminae developed from oxidation spots. III: Cavity forms with twinned patterns of destructively interfered waves. Dotted lines = traces of twinned waves, double-sided arrows = wave period, numbered double-sided arrows 1 and 2 = low- and high-frequency waves, respectively, joined arrows = twinned waves, white arrows = initial oxidation spots.

Figure 3. Petrography of quartz botryoids. Barberton cherts: I) OM-rich build-up with radial acicular quartz, III) OM-rich circular-concentric laminae with radial quartz, V) Wavy laminae of cryptocrystalline quartz with OM, VII) Chalcocite and Fe-oxides in botryoids. Gunflint chert: II) OM-rich microdigitate stromatolite, IV) Circular concentricity with radial acicular quartz (1), mosaic quartz of radial fabric (2), and microquartz (3), VI) OM-rich stromatolite laminae, VIII) Carbonate and OM interspersed within spheroids. Red lines = radially aligned quartz, red squares = Raman targets for OM peak-fitting, solid squares = Raman-targeted spots linked to their corresponding spectra. Notable peaks: 207–210 and 468–469 cm^{-1} (quartz), 282 and 392 cm^{-1} (chalcocite), 453 and 616 cm^{-1} (ferrihydrite), 1091 cm^{-1} (ankerite), 1330–1353 cm^{-1} (D1 band), 1603–1613 cm^{-1} (G band). Note that fluorescence overprints OM spectra in III.

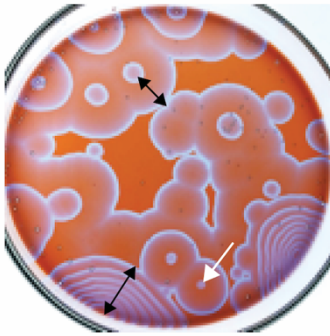
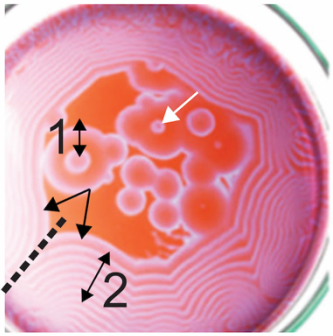
Figure 4. Synoptic models for the diagenetic growth of investigated botryoids from abiotic decarboxylation of biomass.



I)



II)



III)

